

Linear and Nonlinear Optical Propagation in 2D Materials

Nicola Curreli*,¹ Alessandro Fanti,² Giuseppe Mazzeola,² and Ilka Kriegl¹

¹*Functional Nanosystems, Istituto Italiano di Tecnologia, via Morego 30, 16163 Genova, Italy*

²*Department of Electric and Electronic Engineering,
University of Cagliari, Via Marengo 2, 09123 Cagliari, Italy*

Recently, a lot of effort has been dedicated to developing next-generation optoelectronic devices based on two-dimensional materials, thanks to their unique optical properties that are significantly different from those of their bulk counterparts. In order to implement high-performance nanoscale optical devices, an in-depth study of how linear and non-linear propagation occurs in two-dimensional materials is required. Here, we focus on the theory behind the propagation of electromagnetic waves in two-dimensional materials as well as emerging applications in the fields of electronics, optics, sensors, which are summarized and discussed in the paper.

INTRODUCTION

Over the last 15 years, the study of two-dimensional (2D) materials has progressed rapidly in a variety of scientific and engineering subfields [1, 2]. Compared to their conventional bulk counterparts, 2D materials exhibit electronic confinement effects within two dimensions because their thickness is in the order of subnanometers [3–5]. The types of 2D materials available have been continuously growing, including insulators, semiconductors, and a plethora of metals and semimetals [6–22]. Their tunable optical and electronic properties [23–25] and their easy integration allow improving the performance of optoelectronic devices [26–30]. In fact, 2D materials properties are determined by their structural features, in which dimensionality plays a fundamental role [31, 32]. When approaching the two-dimensional nature of crystals, defined as an infinite crystalline in-plane periodic structure with atomic thickness, novel peculiar properties arise [33]. In addition to unique electronic and optical properties, these materials show high mechanical strength and flexibility [34]. The quantum confinement in the direction perpendicular to 2D crystals planes, promote a longer mean free path of electrons, excitons, phonons, and ballistic in-plane transport without scattering or diffusion [31, 35, 36]. Moreover, the 2D geometry is compatible with the design and implementation of optical devices finding application in electronics, optics, and many other fields [37]. For these reasons, in this article, we focus on theoretical and experimental research of linear and non-linear optical propagation and effects caused by different electromagnetic external stimuli in 2D materials.

ELECTRONIC AND OPTICAL PROPERTIES OF 2D MATERIALS

Since the discovery of graphene [38], new materials have been added to the family of 2D materials at an increasing pace. Among them, the most interesting are hexagonal boron nitride (h-BN) [31, 39, 40], transition-

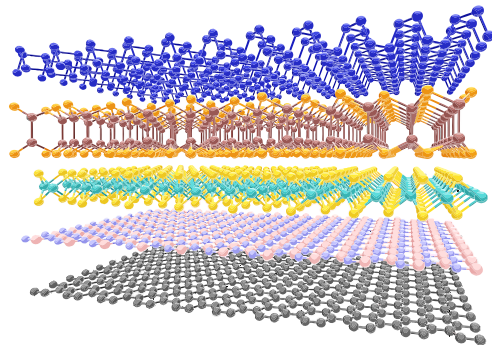


FIG. 1: Sketch of several 2D materials. From top to bottom: phosphorene, InSe, MoS₂, h-BN and graphene.

metal dichalcogenides (TMDs, such as MoS₂, MoSe₂, WS₂, WSe₂) [40, 41], silicene [42, 43], germanene [44], stanene [45], phosphorene [46–48], borophene [49, 50], just to cite few. All of those materials cover the entire spectrum of electrical conductivity from (semi)metals (*e.g.*, graphene and borophene) and semiconductors (*e.g.*, TMDs) to insulators (*e.g.*, h-BN) (Fig. 1).

Graphene

Graphene is a 2D crystal formed by carbon atoms arranged in a hexagonal honeycomb lattice. The electronic structure of graphene can be derived through a tight-binding model, in which Dirac cones are found at the corners of the Brillouin zone (Fig. 2a) [51, 52]. In the proximity of these points, charge carriers obey a linear dispersion relation:

$$E = \pm v_F p \quad (1)$$

where E and p are the energy and the momentum measured with respect to the Dirac points, $v_F = 10^6 \text{ m s}^{-1}$ is the Fermi velocity, while the plus and minus signs refer to the conduction and valence bands, respectively [52]. The bands with conical dispersion intersect at the Fermi energy, thus making graphene a semimetal.

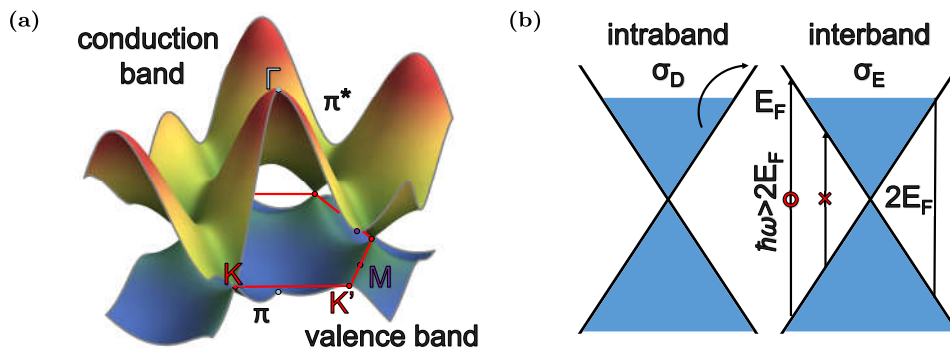


FIG. 2: a) The electronic energy dispersion of graphene throughout the whole region of Brillouin zone. b) The dispersion around K point, on the left the intraband transition of electron while, on the right the interband transition of electron, which occurs if $\hbar\omega > 2E_F$.

As a result, an additional-chiral-symmetry exists, fixing a parallel or antiparallel pseudospin to the directions of motion of the carriers [52, 53]. This contributes to peculiar effects on the electronic and optical properties of graphene. For example, for undoped samples at 0 K the universal optical conductivity of graphene, which links the surface current density \mathbf{J} to the electric field \mathbf{E} ($\mathbf{J} = \bar{\sigma}\mathbf{E}$), is independent of any material parameter:

$$\bar{\sigma}_0 = \frac{e^2}{4\hbar} \sim 6.08 \times 10^{-5} S \quad (2)$$

where e is the electron charge and \hbar is the reduced Planck's constant. Thus, the transmission for a single layer graphene is given as [53–56]:

$$T = (1 + 0.5\pi\alpha)^{-2} \sim 1 - \pi\alpha \sim 97.7\% \quad (3)$$

where $\alpha = e^2/(4\pi\epsilon_0\hbar c) = \bar{\sigma}_0/(\pi\epsilon_0 c) \sim 1/137$ is the fine-structure constant [54, 56]. Notably, the optical absorption depends only on the fine-structure constant, and is given as $A \sim 1 - T \sim \pi\alpha \sim 2.3\%$, considering that for a monolayer the reflection contribution (R) is less than 0.1% (Fig. 3) [56]. On the other hand, doping has a strong effect on optical properties [53, 57], because of the so-called Pauli blocking [53]. In fact, Pauli blocking ensures that photons with energy ($\hbar\omega$) less than $2E_F$ (where E_F is the Fermi energy) can not be absorbed (Fig. 2b) [52–54, 58].

The conical dispersion of low-energy carriers in graphene is very different from other materials' parabolic dispersion [51, 52]. For example, bilayer graphene presents parabolic dispersion at the Fermi energy and a small bandgap of up to 250 meV that can be opened with an electric field [54, 59, 60]. In the case of multiple layer structures (such as bilayer or few-layer graphene), it is possible to consider an optically equivalent superposition of almost non-interacting single-layer graphene flakes in which each layer can be seen as a 2D electron gas with little perturbation from the adjacent one [61]. For few-layer graphene, the contribution of the reflection

becomes more prominent, reflecting $\sim 2\%$ of the incident light for ten-layer crystals [61].

Frequency-independent absorption of graphene along with extremely high carrier mobility has attracted the interest of the scientific community. A particularly interesting research direction is its use in flexible electronic devices such as touch screens [54], electronic paper, organic photovoltaic cells [62] and organic light-emitting diodes [63], thanks to its flexibility as well as its low surface resistance and high transmittance. Moreover, graphene is used to implement photodetectors that are used in the broadband spectral region between the ultraviolet and infrared [64]. Furthermore, in a single layer of graphene [65], the interband transition photoelectrons are modulated by a driving voltage over a wide band in order to obtain an optical modulator with a bandwidth in the near-infrared region of over 1 GHz [64].

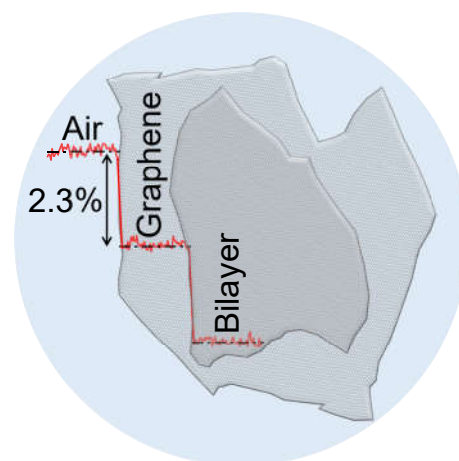


FIG. 3: Schematic of the intensity of transmitted white light through graphene and bilayer graphene. The dashed line scan profile shows the intensity between layers.

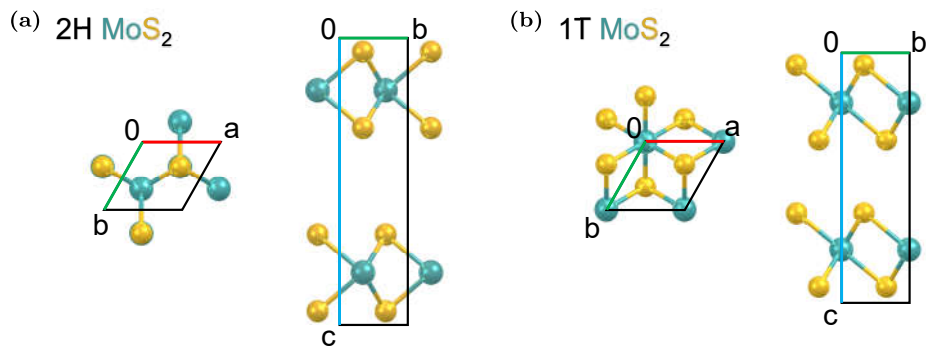


FIG. 4: a) 2H and b) 1T MoS_2 crystal structure.

Transition Metal Dichalcogenide Monolayers

The interesting properties of graphene have led to the discovery and study of other 2D crystals and heterostructures thereof, showing exciting optical properties which differ from their bulk counterparts. Transition metal dichalcogenides (TMDs) are probably the second most-studied 2D material class after graphene. They are a family of materials with MX_2 chemical formula, where M is a transition metal and X is a chalcogen such as S, Se, or Te [41, 51]. The TMDs' atomic and electronic structure consists of a layer of M atoms inserted between two atomic layers of X atoms, with a hexagonal unit cell having D_{3h} symmetry and a thickness of $\sim 0.7 \text{ nm}$ [41, 66–68]. Within the TMDs it is possible to find metallic (*e.g.*, VS_2 and NbS_2), semiconducting (*e.g.*, MoS_2 and WS_2) or insulating (*e.g.*, HfS_2) materials [41, 68]. The TMD crystals show different polyforms [41, 68]. Typical crystal structures include trigonal prismatic 1H (2H for multilayer), 1T, and 1T' (*i.e.*, distorted-1T) phases [33, 37, 69], as shown in Fig. 4. The most stable crystalline configuration is the 2H-stacking (also known as AB-stacking) [41, 51, 70]. In particular, semiconducting 2H TMDs show peculiar optical and electronic properties, fundamentally different from their 3D bulk counterparts. For example, MoS_2 [66, 67, 71], MoSe_2 [51, 72], WS_2 , and WSe_2 [73] undergo a crossover from indirect to direct gap when going from bilayer to monolayer form. In the case of MoS_2 , bulk crystals have an indirect bandgap of the order of 1.29 eV, while in its 2D form, MoS_2 presents a direct bandgap [53, 71] of $\sim 1.9 \text{ eV}$ around the K points of the Brillouin zone. This leads to pronounced luminescence enhancement [66].

Other 2D materials

Similarly, layered post-transition metal chalcogenides of the group-III, such as GaS, GaSe, SnS, SnS_2 , and InSe, are also being explored due to their high mobilities, large photoresponses, and in-plane anisotropy [70, 74]. They

present different polytypes which vary with respect to their layer-stacking configuration, namely, the group-IV monochalcogenides (*e.g.*, SnS and GeSe) [75] or the 1T dichalcogenides (*e.g.*, SnS_2) [70].

Moreover, there is also the family of 2D transition metal carbides, nitrides, and carbonitrides which are known as MXenes with the following chemical formulas: M_2X , M_3X_2 and M_4X_3 , where M is an early transition metal and X is a carbon or a nitrogen atom [76]. They exhibit interesting mechanical properties as well as good thermal and electrical conductivity [70].

In addition, wide bandgap 2D materials play a key role in device implementation. For example, hexagonal boron nitride (h-BN), thanks to its inert nature, insulating characteristics and ultra-flat structure, act as a substrate or sacrificial layer for high-mobility 2D crystal-based devices [77].

Other wide bandgap materials, including transition metal oxides (TMO - *e.g.*, MoO_2 with 2H-phase, MnO_2 with 1T-phase and $\alpha\text{-MoO}_3$) and chromium oxide (*i.e.*, Cr_2O_3), known for its multiferroic properties [78], exhibit hyperbolic optical behavior [70, 79].

Other examples of layered materials include elementary 2D materials, such as phosphorus allotropes (*e.g.*, black and blue phosphorus) [47], silicene [80], germanene [81], tellurene [82], gallene [83], antimonene [84], and borophene [85], which range from metallic to semiconductor as well as topological insulators (for example, Bi_2Se_3 and Sb_2Se_3) known for their topologically protected and spin-momentum-locked electronic transport [70, 86].

OPTICAL PROPAGATION IN 2D MATERIALS

In this section, the electromagnetic surface wave [87] that propagates in a direction parallel to the 2D material layer, as well as transmission and reflection of electromagnetic waves by a periodic structure consisting of N layers, will be investigated.

The electromagnetic surface wave in 2D materials

An electromagnetic surface wave is a field configuration essentially confined in a small region close to the interface between two dielectric media and propagating in the direction along the interface itself [88–94]. Here, we consider only plane interfaces and choose a cartesian reference frame with the z -axis normal to the interface (Fig. 5). By our convention, the surface wave propagates in the x -direction and the field decays in the z -direction. The basic principle behind the phenomenon of the surface waves is the solution of Maxwell's equations at the interface. From this, it is possible to obtain that surface waves are excited by external incident electromagnetic waves [88, 94, 95]. Surface plasmon polaritons (SPPs) are a particular type of electromagnetic surface waves traveling along with a metal-dielectric or metal-air interface in the infrared or visible-frequency range. The physical characteristics of SPPs in metals are determined by their intrinsic properties and the geometry of the material. The thickness plays a very important role in the physical propagation of SPPs. In fact, more recently, it has been found that 2D materials, inserted at the interface between dielectrics, support SPPs thanks to the strongly confined electric field as the thickness approaches the atomic level and light is being confined to dimensions 2-3 order of magnitude smaller than that of the free-space wavelength [96]. The polarization of the incident waves determines the polarization of surface waves, therefore it is possible to find transverse magnetic (TM) and transverse electric (TE) surface waves, determining the components of the field for each surface wave. In the TM surface wave, the incident field has a component of a magnetic field perpendicular to the incidence plane (Fig. 5a), while in the TE surface wave, the incident field has a component of an electric field perpendicular to the incidence plane (Fig. 5b).

Field configuration at TM surface wave

For a TM surface wave, E_x , E_z , H_y field components are considered, and it is assumed that the 2D material is surrounded by two dielectric media 1 and 2 as shown in Fig. 5a. The TM surface wave propagates on the surface of the 2D material in the x -direction with wave vector in the direction of propagation ($\vec{q} = q\vec{x}$). In medium 1, the electromagnetic fields of the TM surface wave are given by [88]:

$$\begin{aligned} E_x^{(1)} &= E_1 e^{iqx} e^{-\kappa_1 z} \\ E_z^{(1)} &= \frac{iq}{\kappa_1} E_x^{(1)} \\ H_y^{(1)} &= -\frac{i\omega\varepsilon_0\varepsilon_1}{\kappa_1} E_x^{(1)} \end{aligned} \quad (4)$$

while in medium 2:

$$\begin{aligned} E_x^{(2)} &= E_2 e^{iqx} e^{\kappa_2 z} \\ E_z^{(2)} &= -\frac{iq}{\kappa_2} E_x^{(2)} \\ H_y^{(2)} &= \frac{i\omega\varepsilon_0\varepsilon_1}{\kappa_2} E_x^{(2)} \end{aligned} \quad (5)$$

where $E_x^{(i)}$, $E_z^{(i)}$ and $H_y^{(i)}$ are the electric field in the x , y and z directions respectively, E_i is the amplitude of electric field in the x -direction, for the i^{th} medium ($i = 1, 2$), ε_0 and ε_1 are the dielectric constant of the vacuum and the medium respectively, and κ_i is decay constant of the fields inside the i^{th} medium given by:

$$\kappa_i = \sqrt{q^2 - \omega^2\varepsilon_i/c^2} \quad (6)$$

The magnetic and the electric field are related by the following relations:

$$E_x^{(i)} = -\frac{i}{\omega\varepsilon_0\varepsilon_i} \frac{\partial H_y^{(i)}}{\partial z} \quad (7)$$

$$E_z^{(i)} = -q/(\omega\varepsilon_0\varepsilon_i) H_y^{(i)} \quad (8)$$

which can be derived from Maxwell's equations [88]. Due to the presence of surface currents that flow on the 2D material, the magnetic field components are not continuous. Therefore, the boundary conditions of the electromagnetic wave on the surface of 2D material are given by:

$$E_x^{(1)} = E_x^{(2)} \quad (9)$$

$$H_y^{(1)} - H_y^{(2)} = -J \quad (10)$$

where $J = \vec{\sigma}(\omega)E_x^{(2)}$ is the surface current on the 2D material and $\vec{\sigma}(\omega)$ is the complex optical conductivity of 2D material. Since a 2D material presents a negligible thickness, when compared to the wavelength in the materials, J appears only in the boundary conditions.

In the case of graphene, there are two contributions to $\vec{\sigma}(\omega)$, corresponding to two possible optical scattering or excitation of electron by photon, which are the intraband transition (within the same conduction band) and interband transition (from valence to conduction band), as shown in Fig. 2b. The real and imaginary parts of $\vec{\sigma}(\omega)$ are related by the Kramers-Kronig relation and it is given by the following equation [97–102]:

$$\begin{aligned} \vec{\sigma}(\omega) &\equiv \sigma_D + \text{Re}\{\sigma_E\} + i \text{Im}\{\sigma_E\} = \\ &= \frac{E_F e^2}{\pi\hbar} \frac{i}{\hbar\omega + i\Gamma} + \frac{e^2}{4\hbar} \delta_{-1}(\hbar\omega - 2E_F) + \\ &\quad - \frac{ie^2}{4\pi\hbar} \ln \left| \frac{\hbar\omega + 2E_F}{\hbar\omega - 2E_F} \right| \end{aligned} \quad (11)$$

The first term in Eq. 11 (σ_D) is the intraband conductivity (or Drude conductivity) [99–101], while the second

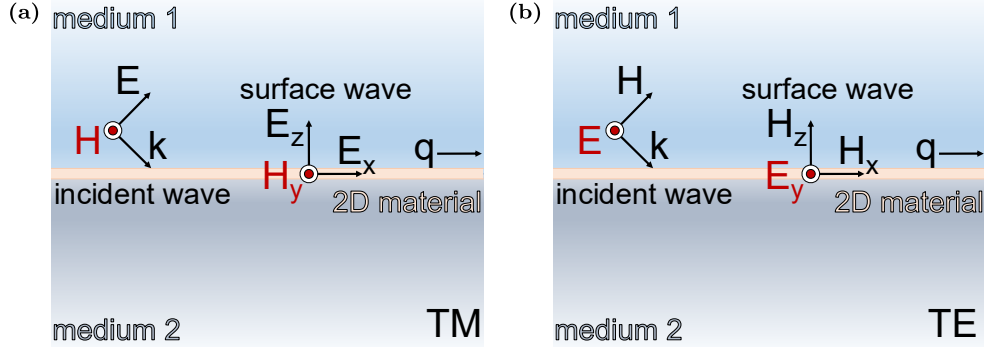


FIG. 5: a) TM surface wave and b) TE surface wave in 2D materials. 2D material is shown as orange color with negligible thickness.

and the third terms correspond to the real part and the imaginary part of interband conductivity (σ_E), respectively [97, 99, 101]. The $\delta_{-1}(x)$ is the Heaviside step function, while the spectral width (Γ) is a parameter that describes the scattering rate with phonons due to the impurities and depends on the Fermi level (E_F) as:

$$\Gamma = \hbar v_F^2 / \mu E_F \quad (12)$$

where $v_F = 10^6$ m/s is the Fermi velocity of graphene and $\mu = 10^4$ cm²/Vs is the mobility for ideal graphene [100]. For $\hbar\omega < 2E_F$ the intraband transition is dominant and the optical transition of the electron with $q \neq 0$ is possible, due to the additional scattering of an electron by impurity or phonon, which might modify the momentum of the electron. On the other hand, the interband transition from the valence to conduction band is dominant for $\hbar\omega > 2E_F$ [101]. For a 2D electron gas system (e.g., GaAs/AlGaAs quantum-well structure), the optical conductivity is described by [97, 103]:

$$\bar{\sigma}_{2Dgas} = i \frac{ne^2}{m(\omega + i\gamma)} \quad (13)$$

where n , m and γ are the density, effective mass, and scattering rate of the 2D electron gas system. The dispersion of TM surface wave is obtained by substituting Eqs. 4-5 to boundary conditions (Eqs. 9 and 10). In addition, the following equation is a requirement to have TM surface wave in the 2D material [97, 99, 100, 104]:

$$\frac{\varepsilon_1}{\kappa_1} + \frac{\varepsilon_2}{\kappa_2} + \frac{i\bar{\sigma}(\omega)}{\omega\varepsilon_0} = 0 \quad (14)$$

where ε_i , ($i = 1, 2$) is the dielectric constant of the i^{th} medium, which surrounds the 2D material. Considering that $\varepsilon_i > 0$ and $\kappa_i > 0$. In order to satisfy Eq. 14, the imaginary part of $\bar{\sigma}(\omega)$ should be positive ($\text{Im}\{\bar{\sigma}(\omega)\} > 0$). This requirement is satisfied by the conventional 2D electron gas system, since $\text{Im}\{\bar{\sigma}_{2Dgas}\} = ne^2\omega / (m(\gamma^2 + \omega^2)) > 0$ [97], and in the case of graphene $\text{Im}\{\bar{\sigma}(\omega)\} > 0$ for $\hbar\omega < 1.667E_F$. By solving Eq. 14, it is possible

to derive the dispersion relation of TM surface wave for graphene. If $\hbar\omega \ll 2E_F$ (being $E_F = 0.64$ eV), it is obtained that $\bar{\sigma}(\omega) \sim \sigma_D(\omega)$ and Γ can be ignored, since it gives only the spectral broadening of the TM surface wave. When the velocity of light can be considered to be much larger than the group velocity of surface plasmon v_{sp} , thus $q \gg \omega/c$ obtaining $\kappa_1 = \kappa_2 = q$ in Eq. 6 this condition is called the non-retarded regime [93, 100, 105]. By substituting σ_D in Eqs. 11 to Eq. 14 and solve for ω , a square-root dependence ($\omega \propto \sqrt{q}$) of the dispersion relation is obtained [93, 100, 105, 106]:

$$\omega = \frac{1}{\hbar} \sqrt{\frac{E_F e^2 q}{\pi \varepsilon_0 (\varepsilon_1 + \varepsilon_2)}} \quad (15)$$

The aforementioned relation can be also obtained for conventional 2D electron gas by substituting Eq. 13 to Eq. 14, solving for ω , finding that $\omega \propto \sqrt{q}$ dependence is a characteristic of SPP in 2D materials [93, 98, 100, 105]. Considering graphene as a medium, the long-wavelength plasmon dispersion can be calculated by looking for zeros of the dynamical dielectric function ($\varepsilon_g(q, \omega) = 0$) [98, 105].

Field configuration at TE surface wave

For a TE surface wave (Fig. 5b), the field components are E_y , H_x , H_z . In medium 1, the electromagnetic fields of the TE surface wave are given by:

$$\begin{aligned} H_x^{(1)} &= H_1 e^{iqx} e^{-\kappa_1 z} \\ H_z^{(1)} &= \frac{iq}{\kappa_1} H_x^{(1)} \\ E_y^{(1)} &= \frac{i\omega\mu_0}{\kappa_1} H_x^{(1)} \end{aligned} \quad (16)$$

and in medium 2:

$$\begin{aligned} H_x^{(2)} &= H_2 e^{iqx} e^{\kappa_2 z} \\ H_z^{(2)} &= -\frac{iq}{\kappa_2} H_x^{(2)} \\ E_y^{(2)} &= -\frac{i\omega\mu_0}{\kappa_2} H_x^{(2)} \end{aligned} \quad (17)$$

where μ_0 is the permeability of the vacuum. Similarly for the TM surface wave, the magnetic and the electric field are related by the following relations:

$$H_x^{(i)} = \frac{i}{\omega\mu_0} \frac{\partial E_y^{(i)}}{\partial z} \quad (18)$$

$$H_z^{(i)} = q/(\omega\mu_0) E_y^{(i)} \quad (19)$$

and, by using the boundary conditions of the electromagnetic field at the surface $z = 0$, which are related to the case of TM surface wave given in Eqs. 9 and 10:

$$E_y^{(1)} = E_y^{(2)} \quad (20)$$

$$H_x^{(1)} - H_x^{(2)} = -J \quad (21)$$

at $z = 0$, where $J = \bar{\sigma}(\omega) E_y^{(2)}$ and assuming that the two dielectric media as vacuum ($\varepsilon_1 = \varepsilon_2 = 1$, thus $\kappa_1 = \kappa_2 = \sqrt{q^2 - (\omega/c)^2} \equiv \kappa$, it is obtained the following equation [97, 107]:

$$2 - \frac{i\bar{\sigma}(\omega)\omega\mu_0}{\kappa} = 0 \quad (22)$$

The concepts of surface plasmon dispersion and the non-retarded regime [100, 105] have been introduced in Eq. 14 and Eq. 15. For small q , the non-retarded approximation cannot be used because the group velocity of surface plasmon (v_{sp}) is comparable to the velocity of light. This case is the so-called retarded regime [105], in which the dispersion of surface plasmon is linear ($\omega \propto q$). From Eq. 6 and solving Eq. 14, supposing that $\varepsilon_1 = \varepsilon_2 = \varepsilon$, for retarded regime it has been obtained:

$$\omega \sim \frac{c}{\sqrt{\varepsilon}} q \quad (23)$$

For a conventional 2D electron gas system, $\text{Im}\{\bar{\sigma}_{2Dgas}\} > 0$, as given by Eq. 13 [97], hence, the TE surface wave cannot be supported by a normal bulk metal or any other common material found in nature, since $\omega > 0$, and Eq. 23 requires $\text{Im}\{\bar{\sigma}\} < 0$ [89, 97]. However, it is possible to obtain artificial materials that possess a negative permeability (*e.g.*, metamaterials [108] - generally not easy to fabricate - and 2D materials [109]). For example, in the case of graphene, $\text{Im}\{\bar{\sigma}(\omega)\} < 0$ for $\hbar\omega < 2E_F$. This unusual property has enabled graphene to have the TE surface wave, although TE surface wave in doped graphene occurs only for a narrow frequency range of $1.667E_F < \hbar\omega < 2E_F$ [89, 97, 99, 110].

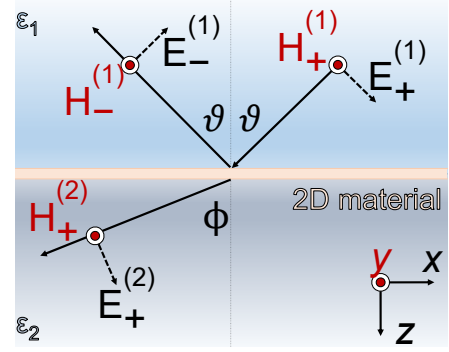


FIG. 6: A 2D material is placed between two dielectric media with dielectric constants ε_1 and ε_2 . The thickness of the 2D material is neglected. The incident EM wave comes at an angle ϑ in medium 1 (top) and is transmitted at an angle ϕ in medium 2 (bottom).

The optical absorption, reflection, and transmission spectra in 2D materials

To describe the optical spectra of the electromagnetic wave incident on a 2D material, Maxwell's equations with boundary conditions were first evaluated, considering the 2D material between two dielectric media. Subsequently, using the transfer matrix method, optical spectra were obtained in the case of a 2D material within a multilayer of dielectric media.

2D material between two dielectric media

The probabilities for absorption, reflection, and transmission of an electromagnetic wave penetrating 2D materials can be obtained by solving Maxwell's equations for an electromagnetic wave with boundary conditions. A 2D material, having a negligible thickness, is placed between two dielectric media as shown in Fig. 6. It is modeled as a conducting interface with a conductivity $\bar{\sigma}$ between two dielectric media with dielectric constants ε_1 and ε_2 . Considering the TM polarization of electromagnetic wave, as shown in Fig. 6, it is possible to obtain two boundary conditions for the electric field $E^{(i)}$ and magnetic field $H^{(i)}$ ($i = 1, 2$) as follows:

$$E_+^{(1)} \cos \vartheta + E_-^{(1)} \cos \vartheta = E_+^{(2)} \cos \phi \quad (24)$$

$$H_+^{(2)} - (H_+^{(1)} - H_-^{(1)}) = -\bar{\sigma} E_+^{(2)} \cos \phi \quad (25)$$

where +(-) index is the bottom- (top-) going waves according to Fig. 6, ϑ is the incident and reflection angle, and ϕ is the refraction angle. The E and H fields are related to each other in terms of the electromagnetic wave impedance, for each medium:

$$Z_i = \frac{E_i}{H_i} = \frac{377}{\sqrt{\varepsilon_i}} \Omega \quad (i = 1, 2) \quad (26)$$

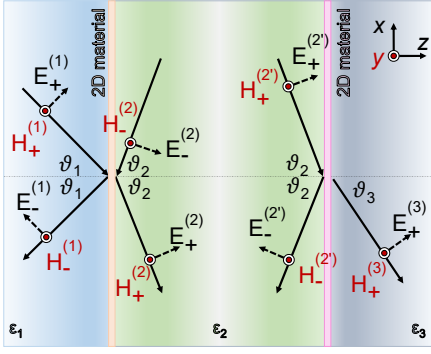


FIG. 7: The wave propagation through three media and two different 2D materials.

where the constant 377Ω is the impedance of vacuum ($Z_0 = \sqrt{\mu_0/\epsilon_0}$). Quantities ϕ , ϑ , and Z_i are related by Snell's law ($Z_2 \sin \vartheta = Z_1 \sin \phi$). Solving Eqs. 24-26, reflection (R), transmission (T), and absorption (A) probabilities of the electromagnetic wave are obtained as follows:

$$\begin{aligned}
 R &= \left| \frac{E_1^{(-)}}{E_1^{(+)}} \right|^2 = \\
 &= \left| \frac{Z_2 \cos \phi - Z_1 \cos \vartheta - Z_1 Z_2 \bar{\sigma} \cos \vartheta \cos \phi}{Z_2 \cos \phi + Z_1 \cos \vartheta + Z_1 Z_2 \bar{\sigma} \cos \vartheta \cos \phi} \right|^2 \\
 T &= \frac{\cos \phi Z_1}{\cos \vartheta Z_2} \left| \frac{E_2^{(+)}}{E_1^{(+)}} \right|^2 = \\
 &= \frac{4Z_1 Z_2 \cos \vartheta \cos \phi}{|Z_2 \cos \phi + Z_1 \cos \vartheta + Z_1 Z_2 \bar{\sigma} \cos \vartheta \cos \phi|^2} \\
 A &= 1 - \text{Re}\{R\} - \text{Re}\{T\} = \\
 &= \frac{4Z_1 Z_2^2 \cos \vartheta |\cos \phi|^2 \text{Re}\{\bar{\sigma}\}}{|Z_2 \cos \phi + Z_1 \cos \vartheta + Z_1 Z_2 \bar{\sigma} \cos \vartheta \cos \phi|^2} \quad (27)
 \end{aligned}$$

where the values of R , T , and A are real quantities and are denoted in terms of percentage (0 – 100%).

Multilayer configuration

The configuration described in the previous section can be generalized to a multilayer configuration in which 2D and standard dielectric slabs alternate. This structure can be modeled using the formalism of the equivalent chain of transmission lines [111], and then analyzed using the wave-amplitude transmission matrix (WATM) [112]. The latter is very effective when, as in our case, we are mainly interested in an input-output description of the structure and has already been used in the present context [113–115]. Assuming N 2D materials inside a multilayer dielectric media spaced from each other by a dis-

tance $z = d$, the WATM method [116] relates the electromagnetic fields at all interfaces in a multi-layered system. For simplicity, a system with two 2D material layers placed between three dielectric slabs (medium 1, 2 and 3 with dielectric constants ϵ_1 , ϵ_2 and ϵ_3 , respectively), can be assumed as a first approximation (Fig. 7). The incident electromagnetic wave with TM polarization comes from medium 1 with angle ϑ_1 and it propagates through medium 2 with angle ϑ_2 and medium 3 with angle ϑ_3 . By adopting the polarization TM of the incident electromagnetic wave, between two dielectric media ($0 < z < d$), the electromagnetic fields are related to each other through the boundary conditions obtained from Maxwell's equations. Therefore, it is possible to define the boundary conditions of the monolayer interface of the electric field $E^{(i)}$ and of the magnetic field $H^{(i)}$ ($i = 1, 2$) as follows:

$$E_x^{(1)} = E_x^{(2)} \quad (28)$$

$$H_y^{(2)} - H_y^{(1)} = -\bar{\sigma} E_x^{(2)} \quad (29)$$

Considering a thickness of the 2D material sufficiently small compared to the wavelength of the incident light ($d \ll \lambda$), the electric and magnetic fields in medium 1 can be described as follows:

$$\begin{aligned}
 E_x^{(1)}(z) &= E_{x_+}^{(1)}(z) + E_{x_-}^{(1)}(z) = \\
 &= E_{x_0+}^{(1)} e^{i\kappa_1 z} + E_{x_0-}^{(1)} e^{-i\kappa_1 z} \quad (30)
 \end{aligned}$$

$$H_y^{(1)}(z) = \frac{\omega \epsilon_0 \epsilon_1}{\kappa_1} (E_{x_0+}^{(1)} e^{i\kappa_1 z} - E_{x_0-}^{(1)} e^{-i\kappa_1 z}) \quad (31)$$

and for medium 2:

$$\begin{aligned}
 E_x^{(2)}(z) &= E_{x_+}^{(2)}(z) + E_{x_-}^{(2)}(z) = \\
 &= E_{x_0+}^{(2)} e^{i\kappa_2 z} + E_{x_0-}^{(2)} e^{-i\kappa_2 z} \quad (32)
 \end{aligned}$$

$$H_y^{(2)}(z) = \frac{\omega \epsilon_0 \epsilon_1}{\kappa_2} (E_{x_0+}^{(2)} e^{i\kappa_2 z} - E_{x_0-}^{(2)} e^{-i\kappa_2 z}) \quad (33)$$

where $E_x^{(i)}$ is the amplitude of the electric field along the x -axis inside medium i , ϵ_i is the dielectric constant of the i^{th} medium, ω is the angular frequency of the electromagnetic wave and k_i is the wave vector on z -direction which is defined as:

$$k_i = \frac{2\pi}{\lambda} \sqrt{\epsilon_i} \cos \vartheta_i \quad (34)$$

where λ is the wavelength of the electromagnetic wave. The amplitude of electric field of the electromagnetic wave are $E_{x_0+}^{(i)}$ and $E_{x_0-}^{(i)}$ going to the z -direction. The reflected wave at the second interface with medium 3 inside the medium 2 is described by $E_{x_0-}^{(2)}$. The relationship between H_y and E_x comes from the following equation:

$$H_y^{(i)} = i\omega \epsilon_0 \epsilon_i \int E_x^{(i)} dz \quad (35)$$

The corresponding angle of propagation of the electromagnetic wave inside each dielectric medium measured

from the z -axis is ϑ_i ($i = 1, 2$). Quantities ϑ_i and ε_i between two dielectric media are related by the Snell's law ($\varepsilon_1 \sin \vartheta_1 = \varepsilon_2 \sin \vartheta_2$). Using Eq. 28 through 33, by solving for $E_{x_{0+}}$ and $E_{x_{0-}}$ at the boundary explicitly, it is possible to write the following matrix:

$$\begin{bmatrix} E_{x_{0+}}^{(1)} \\ E_{x_{0-}}^{(1)} \end{bmatrix} = [M_1] [T_1] [M_2] [T_2] \dots [T_{N-2}] [M_{N-1}] \begin{bmatrix} E_{x_{0+}}^{(N)} \\ 0 \end{bmatrix} \quad (36)$$

where:

$$M_i = \frac{1}{2} \begin{bmatrix} 1 + \Delta_i + G_i & 1 - \Delta_i + G_i \\ 1 - \Delta_i - G_i & 1 + \Delta_i - G_i \end{bmatrix} \quad (37)$$

$$T_i = \begin{bmatrix} e^{-i\kappa_{i+1}d} & 0 \\ 0 & e^{i\kappa_{i+1}d} \end{bmatrix} \quad (38)$$

Eq. 37 describes the electromagnetic waves in medium i as a function of the electromagnetic waves in medium $i + 1$ at the first boundary, where α_i and β_i are:

$$G_i = \frac{\kappa_i \bar{\sigma}}{\omega \varepsilon_0 \varepsilon_i}, \quad \Delta_i = \frac{\kappa_i}{\kappa_{i+1}} \frac{\varepsilon_{i+1}}{\varepsilon_i} \quad (39)$$

Eq. 38 describes the propagation of the wave through the medium $i + 1$, where d is the length of the medium $i + 1$.

The total reflection (ρ_{total}) and transmission (τ_{total}) coefficients are:

$$\begin{bmatrix} E_{x_{0+}}^{(1)} \\ E_{x_{0-}}^{(1)} \end{bmatrix} = \begin{bmatrix} \xi & \zeta \\ \gamma & \delta \end{bmatrix} \begin{bmatrix} E_{x_{0+}}^{(3)} \\ 0 \end{bmatrix} \quad (40)$$

$$\rho_{total} = \frac{E_{x_{0-}}^{(1)}}{E_{x_{0+}}^{(1)}} = \frac{\gamma}{\xi}, \quad \text{and} \quad \tau_{total} = \frac{E_{x_{0+}}^{(3)}}{E_{x_{0+}}^{(1)}} = \frac{1}{\xi} \quad (41)$$

where ξ , ζ , γ and δ are the components of total matrix (Eq. 36), getting:

$$\begin{aligned} R &= |\rho_{total}|^2 \\ T &= \frac{\sqrt{\varepsilon_3} \cos \vartheta_1}{\sqrt{\varepsilon_1} \cos \vartheta_3} |\tau_{total}|^2 \\ A &= 1 - \text{Re}\{R\} - \text{Re}\{T\} \end{aligned} \quad (42)$$

where R , T , and A are reflection, transmission, and absorption probabilities of the electromagnetic wave, respectively. In the case of the absence of a 2D material at the interface, $\alpha_i = 0$ can be set in the matching matrix of the corresponding interface.

With this theoretical background, it is possible to optimize the design of optical devices (*e.g.*, optical absorbers). For example, considering a device consisting of N 2D materials and respective media, the number and position of the absorption peaks can be tuned a priori, thus providing the theoretical basis for the study and design of the device and its application.

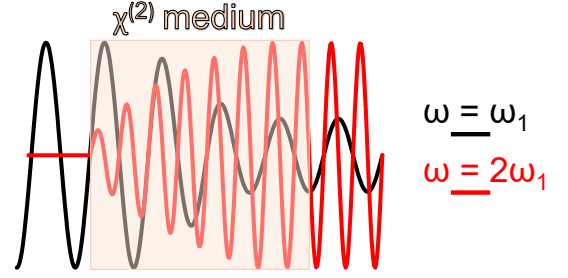


FIG. 8: Diagram of second-harmonic generation with perfect phase matching.

Nonlinear optics in 2D materials

In the previous section, we discussed optical propagation in a 2D material. We have dealt with the problem of a linear dielectric medium impinged by an electromagnetic wave. In this context, a linear dielectric medium is characterized by a linear relation between the polarization density (P) and the electric field (E) [117]:

$$P = \varepsilon_0 \chi E \quad (43)$$

where ε_0 is the permittivity of free space and χ is the electric susceptibility of the medium. The relation between P and E expressed by Eq. 43 describes the conventional linear optical effects, such as refraction and absorption and occurs when E is small, however, it becomes nonlinear when E acquires values comparable to interatomic electric fields, which are typically $\sim 10^5 - 10^8 \text{ Vm}^{-1}$. Since externally applied optical electric fields are typically small in comparison with characteristic interatomic or crystalline fields, even when focused laser light is used, the nonlinearity is usually weak. A nonlinear anisotropic dielectric medium is characterized by a tensor relation which can be expanded in a Taylor series [117]:

$$P_i = \varepsilon_0 \left(\sum_j \chi_{ij} E_j + \sum_{jk} \chi_{ijk}^{(2)} E_j E_k + \sum_{jkl} \chi_{ijkl}^{(3)} E_j E_k E_l + \dots \right) \quad (44)$$

where $i, j, k, l = 1, 2, 3$ and the coefficients χ_{ij} , $\chi_{ijk}^{(2)}$ and $\chi_{ijkl}^{(3)}$ represent the tensor components of the n^{th} -order nonlinearity. These coefficients are characteristic constants of the medium and may be originated by microscopic or macroscopic phenomena. In particular, the $\chi^{(2)}$ coefficient of the second term in Eq. 44, gives rise to second-order nonlinearity (three wave mixing), including second harmonic generation (SHG), sum and difference frequency generation (SFG, DFG), and optical parametric interaction (optical parametric amplification - OPA and optical parametric oscillation - OPO). Third order

nonlinear effects, which usually arise from the susceptibility of third-order nonlinear optics ($\chi^{(3)}$), include third-harmonic generation (THG), four-wave mixing (FWM), intensity-dependent refractive index change (optical Kerr effect and saturable absorption - SA) and two-photon excitation fluorescence (TPEF). The higher order coefficients ($\chi^{(n)}$), represent the susceptibility of high-order nonlinear optics, namely the high-order multiphoton scattering/absorption/luminescence and the high-harmonic generation (HHG). Since the interaction intensity of nonlinear processes usually decreases with n [118, 119], the effects of nonlinear higher-order effects (including HHG) have very low intensity, therefore typically $\chi^{(n)} \sim 0$ for $n > 3$. In the case of bulk crystals, the generation of nonlinear effects occurs when the phase-matching condition is satisfied, in order to maximize the intensity of the nonlinear optical signal. According to quantum mechanics, the phase-matching condition is satisfied when the photon's momentum and energy are simultaneously conserved before and after the nonlinear process [119]. For this reason, the path of the incident light and the orientation of the crystal must be carefully designed in order to optimize the non-linear effects [120]. However, in the case of a medium with reduced thickness, comparable to the sub-wavelength range, and shorter than the coherence length, the phase matching condition is easily achieved. This allows obtaining strong nonlinear effects [120]. Furthermore, the crystalline structure of the material strongly influences nonlinear processes. In fact, thanks to the high values of the tensors $\chi^{(2)}$ and $\chi^{(3)}$, some materials show an anisotropic nonlinear response [121] even if the linear optical response is isotropic. This allows characterizing the orientation of the crystal with very high sensitivity [118, 119].

Since the susceptibility $\chi^{(2)}$ is a third-rank tensor of even parity under inversion, $\chi^{(2)}$ vanishes for media with inversion symmetry. Namely, in centrosymmetric media, which have inversion symmetry, the properties of the medium are not altered by the transformation $\mathbf{r} \rightarrow -\mathbf{r}$ [117]; the $\mathbf{P} - \mathbf{E}$ function must have odd symmetry so that the reversal of E results in the reversal of P without any other change:

$$\begin{aligned} \mathbf{P} &= \varepsilon_0 \left(\chi \mathbf{E} + \chi^{(2)} \mathbf{E}^2 + \chi^{(3)} \mathbf{E}^3 \right) = \\ &= \varepsilon_0 \left(\chi(-\mathbf{E}) + \chi^{(2)}(-\mathbf{E})^2 + \chi^{(3)}(-\mathbf{E})^3 \right) = \\ &= -\mathbf{P} \end{aligned} \quad (45)$$

In order to verify the latter, the second-order nonlinear susceptibility coefficient must be zero ($\chi^{(2)} = 0$). In contrast, odd-order nonlinearity (*i.e.* $\chi^{(3)}$) is allowed in any material, regardless of whether the material is centrosymmetric, such as THG and FWM [119].

Given a plane wave of amplitude $E(\omega)$ traveling in a nonlinear medium (in this case a non-centrosymmetric 2D material) in the direction of its q vector (Fig. 8),

a polarization is generated at the second-harmonic frequency as follows:

$$P(2\omega) = \varepsilon_0 \chi^{(2)} E^2(\omega) = 2\varepsilon_0 d_{\text{eff}} E^2(\omega) \quad (46)$$

where d_{eff} is the effective nonlinear optical coefficient which depends on $\chi^{(2)}$.

If the slowly varying envelope approximation is applied [122]:

$$\left| \frac{\partial^2 E(z, \omega)}{\partial z^2} \right| \ll k \left| \frac{\partial E(z, \omega)}{\partial z} \right| \quad (47)$$

and assuming negligible losses, the wave equation at 2ω is:

$$\frac{\partial E(z, 2\omega)}{\partial z} = -\frac{i\omega}{n_{2\omega}c} d_{\text{eff}} E^2(z, \omega) e^{i\Delta qz} \quad (48)$$

where $\Delta q = q(2\omega) - 2q(\omega)$. Considering the low conversion efficiency assumption ($E(2\omega) \ll E(\omega)$), which is a valid condition when the conversion to the second harmonic is not significant, the amplitude $E(\omega)$ remains constant over the thickness of the nonlinear medium, t . Hence, by using the boundary condition $E(2\omega, z = 0) = 0$, we get:

$$\begin{aligned} E(2\omega, z = t) &= -\frac{i\omega}{n_{2\omega}c} d_{\text{eff}} E^2(z, \omega) \int_0^t e^{i\Delta qz} dz = \\ &= -\frac{i\omega}{n_{2\omega}c} d_{\text{eff}} E^2(\omega) t \frac{\sin(\frac{1}{2}\Delta qt)}{\frac{1}{2}\Delta qt} e^{\frac{i}{2}\Delta qt} \end{aligned} \quad (49)$$

In terms of the optical intensity:

$$I(2\omega, t) = |E(2\omega, t)|^2 = \frac{2\omega^2 d_{\text{eff}}^2 t^2}{n_{2\omega} n_{\omega}^2 c^3 \varepsilon_0} \left(\frac{\sin(\frac{1}{2}\Delta qt)}{\frac{1}{2}\Delta qt} \right)^2 I^2(\omega) \quad (50)$$

The intensity $I(2\omega)$ is maximized for the phase-matched condition $\Delta q = 0$. The Eq. 50 shows that $I(2\omega, t) = 0$ when $d_{\text{eff}} \propto \chi^{(2)} = 0$ for media presenting inversion symmetry. For example, the natural vertical stacking of the most commonly used transition metal dichalcogenide semiconductors - TMDS (2H polytype), is constituted by monoatomic layers rotated by 180° with respect to their next neighbors, forming the so-called AB stack [123]. As a direct consequence, the inversion symmetry is present for even layers ($\chi^{(2)} = 0$), preventing the observation of any second-order nonlinear process [124]. However, TMDS can be reduced to nanometric thickness ($t \sim 1 \text{ nm}$) due to the weak van der Waals interlayer forces, showing a non-centrosymmetric structure ($\chi^{(2)} \neq 0$) in their monolayer form. In this case, the medium is usually presented without any phase factor ($\Delta q = 0$) due to the atomically thin nature [125, 126], hence:

$$E(2\omega) = -\frac{i\omega}{n_{2\omega}c} d_{\text{eff}} E^2(\omega) t \quad (51)$$

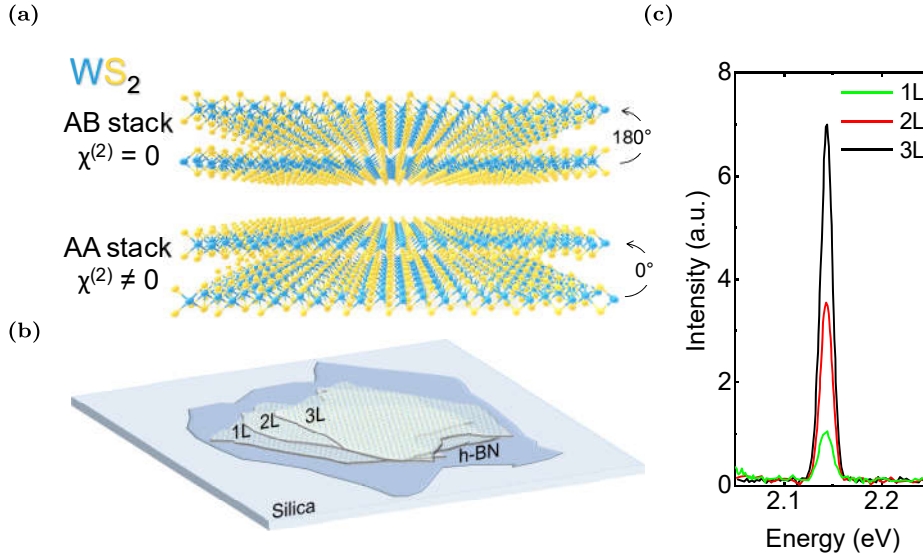


FIG. 9: a) Schematics of natural centrosymmetric AB structure with an interlayer twist angle of 180° ($\chi^{(2)} = 0$) and artificial non-centrosymmetric AA configuration with 0° twist angle ($\chi^{(2)} \neq 0$). b) Sketch of the WS₂ AA stack sample. c) Photoluminescence spectra from as a function of the number of layers. Data from ref. [122].

However, the crystal structure is very important for symmetry reasons and it is possible to find bulk crystals of TMDS possessing a $\chi^{(2)} \neq 0$. For example, in ref. [126] the authors probe the SHG generated from the noncentrosymmetric $3R$ crystal phase of MoS₂. Instead Trovatiello et. al., in ref. [122] show that artificial crystals with vertically stacked WS₂ monolayers, with interlayer $\sim 0^\circ$ crystal angle alignment, forming the so-called AA stack [123], preserve the broken inversion symmetry ($\chi^{(2)} \neq 0$), as shown in Fig. 9a. In both cases, if no strong interactions are assumed between the layers and each layer is treated as optically independent, it is possible to model the individual electric-field from any layer as:

$$E(N, 2\omega) \propto e^{i\Delta q(N-1)t} e^{-\alpha(N-1)t/2} \quad (52)$$

where N is the number of the layers and $(N - 1)$ results due to the indexing of the crystal, *i.e.*, the top-most layer is 1, so the subsequent intensity is normalized to 1, and t is the crystal thickness. To account for the re-absorption of the second harmonic light, it is introduced an exponential loss factor, α . This is the attenuation factor at the second harmonic energy extracted from the single-layer linear absorption spectrum (*i.e.*, $\gamma = 1 - I_{abs} = e^{-\alpha t}$). It is possible to write the total SH light from N layers as:

$$I(N, 2\omega) \propto \left| \sum_{M=1}^N e^{i\Delta q(M-1)t} e^{-\alpha(M-1)t/2} \right|^2 \quad (53)$$

From Eq. 53, it is clear that the intensity scales quadratically with N in the case of a non-centrosymmetric crystal of N layers. This has been observed experimentally, performing a proof-of-principle demonstration. As shown

in Fig. 9b, three layers of manually AA stacked WS₂ sitting on top of a h-BN flake, have been identified by photoluminescence characterization, demonstrating that artificial stacking of AA aligned WS₂ monolayers provides a route for quadratic scaling of the efficiency with layers' number (Fig. 9c).

CONCLUSION

2D materials offer compelling perspectives for implementing devices with new capabilities over those based on conventional materials. In non-interacting 2D material layers, the transfer matrix method can be used to obtain their reflectance, transmittance, and absorbance spectra. In this way, photonic band structures for periodic 2D material layers can be studied in a simple way. Another key feature of 2D non-linear materials is their non-centrosymmetry, which can be easily realized in 2D materials. For example, WS₂ becomes non-centrosymmetric when its bulk counterpart is thinned into a monolayer. These properties demonstrate that these effects greatly improve performance in 2D material-based devices. Hence, it is of great importance to pursue appropriate 2D crystals without thickness limitation, which can provide more opportunities to obtain high-performance optoelectronic devices. All this research paves the way for optical devices ranging from sensors to modulators to isolators, serving as a versatile tool to study optical properties in 2D materials.

-
- [1] Konstantin S Novoselov and AK Geim. The rise of graphene. *Nat. Mater.*, 6(3):183–191, 2007.
- [2] Andrea C Ferrari, Francesco Bonaccorso, Vladimir Fal’Ko, Konstantin S Novoselov, Stephan Roche, Peter Bøggild, Stefano Borini, Frank HL Koppens, Vincenzo Palermo, Nicola Pugno, et al. Science and technology roadmap for graphene, related two-dimensional crystals, and hybrid systems. *Nanoscale*, 7(11):4598–4810, 2015.
- [3] Haotian Wang, Hongtao Yuan, Seung Sae Hong, Yanbin Li, and Yi Cui. Physical and chemical tuning of two-dimensional transition metal dichalcogenides. *Chemical Society Reviews*, 44(9):2664–2680, 2015.
- [4] Qijie Ma, Guanghui Ren, Kai Xu, and Jian Zhen Ou. Tunable optical properties of 2d materials and their applications. *Advanced Optical Materials*, 9(2):2001313, 2021.
- [5] Andrew J Mannix, Brian Kiraly, Mark C Hersam, and Nathan P Guisinger. Synthesis and chemistry of elemental 2d materials. *Nature Reviews Chemistry*, 1(2):1–14, 2017.
- [6] Zhi Wei Seh, Kurt D Fredrickson, Babak Anasori, Jakob Kibsgaard, Alaina L Strickler, Maria R Lukatskaya, Yury Gogotsi, Thomas F Jaramillo, and Aleksandra Vojvodic. Two-dimensional molybdenum carbide (mxene) as an efficient electrocatalyst for hydrogen evolution. *ACS Energy Letters*, 1(3):589–594, 2016.
- [7] Zhengyang Li, Libo Wang, Dandan Sun, Yude Zhang, Baozhong Liu, Qianku Hu, and Aiguo Zhou. Synthesis and thermal stability of two-dimensional carbide mxene ti_3c_2 . *Materials Science and Engineering: B*, 191:33–40, 2015.
- [8] Patrick Urbankowski, Babak Anasori, Taron Makaryan, Dequan Er, Sankalp Kota, Patrick L Walsh, Mengqiang Zhao, Vivek B Shenoy, Michel W Barsoum, and Yury Gogotsi. Synthesis of two-dimensional titanium nitride ti_4n_3 (mxene). *Nanoscale*, 8(22):11385–11391, 2016.
- [9] Xin Han, Dongyu Xu, Lin An, Chengyi Hou, Yaogang Li, Qinghong Zhang, and Hongzhi Wang. $\text{Wo}_3/\text{g-c}_3\text{n}_4$ two-dimensional composites for visible-light driven photocatalytic hydrogen production. *International Journal of Hydrogen Energy*, 43(10):4845–4855, 2018.
- [10] Hongki Min, EH Hwang, and S Das Sarma. Ferromagnetism in chiral multilayer two-dimensional semimetals. *Physical Review B*, 95(15):155414, 2017.
- [11] Kourosh Kalantar-zadeh and Jian Zhen Ou. Biosensors based on two-dimensional mos2. *Acs Sensors*, 1(1):5–16, 2016.
- [12] Xu Zhang, Jesús Grajal, Jose Luis Vazquez-Roy, Ujwal Radhakrishna, Xiaoxue Wang, Winston Chern, Lin Zhou, Yuxuan Lin, Pin-Chun Shen, Xiang Ji, et al. Two-dimensional mos 2-enabled flexible rectenna for wi-fi-band wireless energy harvesting. *Nature*, 566(7744):368–372, 2019.
- [13] Artur Branny, Santosh Kumar, Raphaël Proux, and Brian D Gerardot. Deterministic strain-induced arrays of quantum emitters in a two-dimensional semiconductor. *Nature communications*, 8(1):1–7, 2017.
- [14] Kailiang Zhang, Yulin Feng, Fang Wang, Zhengchun Yang, and John Wang. Two dimensional hexagonal boron nitride (2d-hbn): synthesis, properties and applications. *Journal of Materials Chemistry C*, 5(46):11992–12022, 2017.
- [15] Ming-Yang Li, Chang-Hsiao Chen, Yumeng Shi, and Lain-Jong Li. Heterostructures based on two-dimensional layered materials and their potential applications. *Materials Today*, 19(6):322–335, 2016.
- [16] Ganesh R Bhimanapati, Zhong Lin, Vincent Meunier, Yeonwoong Jung, Judy Cha, Saptarshi Das, Di Xiao, Youngwoo Son, Michael S Strano, Valentino R Cooper, et al. Recent advances in two-dimensional materials beyond graphene. *ACS nano*, 9(12):11509–11539, 2015.
- [17] Wenshan Zheng, Tian Xie, Yu Zhou, YL Chen, Wei Jiang, Shuli Zhao, Jinxiong Wu, Yumei Jing, Yue Wu, Guanchu Chen, et al. Patterning two-dimensional chalcogenide crystals of bi 2 se 3 and in 2 se 3 and efficient photodetectors. *Nature communications*, 6(1):1–8, 2015.
- [18] Sai S. Sunku, Dorri Halbertal, Rebecca Engelke, Hyobin Yoo, Nathan R. Finney, Nicola Curreli, Guangxin Ni, Cheng Tan, Alexander S. McLeod, Chiu Fan Bowen Lo, Cory R. Dean, James C. Hone, Philip Kim, and D. N. Basov. Dual-gated graphene devices for near-field nano-imaging. *Nano Letters*, 21(4):1688–1693, 2021. doi: 10.1021/acs.nanolett.0c04494. URL <https://doi.org/10.1021/acs.nanolett.0c04494>. PMID: 33586445.
- [19] Nicola Curreli, Michele Serri, Marilena Isabella Zappia, Davide Spirito, Gabriele Bianca, Joka Buha, Leyla Najafi, Zdeněk Sofer, Roman Krahne, Vittorio Pellegrini, and Francesco Bonaccorso. Liquid-phase exfoliated gallium selenide for light-driven thin-film transistors. *Advanced Electronic Materials*, 7(3):2001080, 2021. doi:https://doi.org/10.1002/aelm.202001080. URL <https://onlinelibrary.wiley.com/doi/abs/10.1002/aelm.202001080>.
- [20] Nicola Curreli, Michele Serri, Davide Spirito, Emanuele Lago, Elisa Petroni, Beatriz Martín-García, Antonio Politano, Bekir Gürbulak, Songül Duman, Roman Krahne, et al. Liquid phase exfoliated indium selenide based highly sensitive photodetectors. *Advanced Functional Materials*, 30(13):1908427, 2020.
- [21] Andrea Capasso, Sebastiano Bellani, Alessandro Lorenzo Palma, Leyla Najafi, Antonio Esau Del Rio Castillo, Nicola Curreli, Lucio Cina, Vaidotas Miseikis, Camilla Coletti, Giuseppe Calogero, et al. Cvd-graphene/graphene flakes dual-films as advanced dssc counter electrodes. *2D Materials*, 6(3):035007, 2019.
- [22] Sebastiano Bellani, Elisa Petroni, Antonio Esau Del Rio Castillo, Nicola Curreli, Beatriz Martín-García, Reinier Oropesa-Nuñez, Mirko Prato, and Francesco Bonaccorso. Scalable production of graphene inks via wet-jet milling exfoliation for screen-printed micro-supercapacitors. *Advanced Functional Materials*, 29(14):1807659, 2019.
- [23] Matěj Velický and Peter S Toth. From two-dimensional materials to their heterostructures: an electrochemist’s perspective. *Applied Materials Today*, 8:68–103, 2017.
- [24] Andrei Nemilentsau, Tony Low, and George Hanson. Anisotropic 2d materials for tunable hyperbolic plasmonics. *Physical review letters*, 116(6):066804, 2016.
- [25] Yu Li Huang, Yifeng Chen, Wenjing Zhang, Su Ying Quek, Chang-Hsiao Chen, Lain-Jong Li, Wei-Ting Hsu, Wen-Hao Chang, Yu Jie Zheng, Wei Chen, et al. Bandgap tunability at single-layer molybdenum disulfide grain boundaries. *Nature communications*, 6(1):

- 1–8, 2015.
- [26] Zhizhan Qiu, Maxim Trushin, Hanyan Fang, Ivan Verzhbitskiy, Shiyuan Gao, Evan Laksono, Ming Yang, Pin Lyu, Jing Li, Jie Su, et al. Giant gate-tunable bandgap renormalization and excitonic effects in a 2d semiconductor. *Science advances*, 5(7):eaaw2347, 2019.
- [27] Jiaqi Wang, Zhenzhou Cheng, Zefeng Chen, Xi Wan, Bingqing Zhu, Hon Ki Tsang, Chester Shu, and Jianbin Xu. High-responsivity graphene-on-silicon slot waveguide photodetectors. *Nanoscale*, 8(27):13206–13211, 2016.
- [28] Tianjiao Wang, Shuren Hu, Bhim Chamlagain, Tu Hong, Zhixian Zhou, Sharon M Weiss, and Ya-Qiong Xu. Visualizing light scattering in silicon waveguides with black phosphorus photodetectors. *Advanced Materials*, 28(33):7162–7166, 2016.
- [29] Eunho Lee, Seung Goo Lee, Wi Hyoung Lee, Hyo Chan Lee, Nguyen Ngan Nguyen, Min Seok Yoo, and Kilwon Cho. Direct cvd growth of a graphene/mos2 heterostructure with interfacial bonding for two-dimensional electronics. *Chemistry of Materials*, 32(11):4544–4552, 2020.
- [30] Leiming Wu, Jun Guo, Qingkai Wang, Shunbin Lu, Xiaoyu Dai, Yuanjiang Xiang, and Dianyuan Fan. Sensitivity enhancement by using few-layer black phosphorus-graphene/tmdcs heterostructure in surface plasmon resonance biochemical sensor. *Sensors and Actuators B: Chemical*, 249:542–548, 2017.
- [31] Qunhong Weng, Guodong Li, Xinliang Feng, Kornelius Nielsch, Dmitri Golberg, and Oliver G Schmidt. Electronic and optical properties of 2d materials constructed from light atoms. *Advanced Materials*, 30(46):1801600, 2018.
- [32] Ankur Gupta, Tamilselvan Sakthivel, and Sudipta Seal. Recent development in 2d materials beyond graphene. *Progress in Materials Science*, 73:44–126, 2015.
- [33] Karim Khan, Aysha Khan Tareen, Muhammad Aslam, Renheng Wang, Yupeng Zhang, Asif Mahmood, Zhengbiao Ouyang, Han Zhang, and Zhongyi Guo. Recent developments in emerging two-dimensional materials and their applications. *Journal of Materials Chemistry C*, 8(2):387–440, 2020.
- [34] Qing Hua Wang, Kouros Kalantar-Zadeh, Andras Kis, Jonathan N Coleman, and Michael S Strano. Electronics and optoelectronics of two-dimensional transition metal dichalcogenides. *Nature nanotechnology*, 7(11):699–712, 2012.
- [35] Fengnian Xia, Han Wang, Di Xiao, Madan Dubey, and Ashwin Ramasubramaniam. Two-dimensional material nanophotonics. *Nature Photonics*, 8(12):899–907, 2014.
- [36] Fangxu Yang, Shanshan Cheng, Xiaotao Zhang, Xiaochen Ren, Rongjin Li, Huanli Dong, and Wenping Hu. 2d organic materials for optoelectronic applications. *Advanced Materials*, 30(2):1702415, 2018.
- [37] Mingsheng Xu, Tao Liang, Minmin Shi, and Hongzheng Chen. Graphene-like two-dimensional materials. *Chemical reviews*, 113(5):3766–3798, 2013.
- [38] Kostya S Novoselov, Andre K Geim, Sergei V Morozov, Dingde Jiang, Yanshui Zhang, Sergey V Dubonos, Irina V Grigorieva, and Alexandr A Firsov. Electric field effect in atomically thin carbon films. *science*, 306(5696):666–669, 2004.
- [39] Dmitri Golberg, Yoshio Bando, Yang Huang, Takeshi Terao, Masanori Mitome, Chengchun Tang, and Chunyi Zhi. Boron nitride nanotubes and nanosheets. *ACS nano*, 4(6):2979–2993, 2010.
- [40] Jonathan N Coleman, Mustafa Lotya, Arlene O’Neill, Shane D Bergin, Paul J King, Umar Khan, Karen Young, Alexandre Gaucher, Sukanta De, Ronan J Smith, et al. Two-dimensional nanosheets produced by liquid exfoliation of layered materials. *Science*, 331(6017):568–571, 2011.
- [41] Manish Chhowalla, Hyeon Suk Shin, Goki Eda, Lain-Jong Li, Kian Ping Loh, and Hua Zhang. The chemistry of two-dimensional layered transition metal dichalcogenide nanosheets. *Nature chemistry*, 5(4):263–275, 2013.
- [42] Li Tao, Eugenio Cinquanta, Daniele Chiappe, Carlo Grazianetti, Marco Fanciulli, Madan Dubey, Alessandro Molle, and Deji Akinwande. Silicene field-effect transistors operating at room temperature. *Nature nanotechnology*, 10(3):227–231, 2015.
- [43] Jijun Zhao, Hongsheng Liu, Zhiming Yu, Ruge Quhe, Si Zhou, Yangyang Wang, Cheng Cheng Liu, Hongxia Zhong, Nannan Han, Jing Lu, et al. Rise of silicene: A competitive 2d material. *Progress in Materials Science*, 83:24–151, 2016.
- [44] ME Dávila, Lede Xian, Seymour Cahangirov, Angel Rubio, and Guy Le Lay. Germanene: a novel two-dimensional germanium allotrope akin to graphene and silicene. *New Journal of Physics*, 16(9):095002, 2014.
- [45] Sivacarendran Balendhran, Sumeet Walia, Hussein Nili, Sharath Sriram, and Madhu Bhaskaran. Elemental analogues of graphene: silicene, germanene, stanene, and phosphorene. *small*, 11(6):640–652, 2015.
- [46] Likai Li, Yijun Yu, Guo Jun Ye, Qingqin Ge, Xuedong Ou, Hua Wu, Donglai Feng, Xian Hui Chen, and Yuanbo Zhang. Black phosphorus field-effect transistors. *Nature nanotechnology*, 9(5):372, 2014.
- [47] Han Liu, Adam T Neal, Zhen Zhu, Zhe Luo, Xianfan Xu, David Tománek, and Peide D Ye. Phosphorene: an unexplored 2d semiconductor with a high hole mobility. *ACS nano*, 8(4):4033–4041, 2014.
- [48] Jinbo Pang, Alicja Bachmatiuk, Yin Yin, Barbara Trzebicka, Liang Zhao, Lei Fu, Rafael G Mendes, Thomas Gemming, Zhongfan Liu, and Mark H Rummeli. Applications of phosphorene and black phosphorus in energy conversion and storage devices. *Advanced Energy Materials*, 8(8):1702093, 2018.
- [49] Andrew J Mannix, Xiang-Feng Zhou, Brian Kiraly, Joshua D Wood, Diego Alducin, Benjamin D Myers, Xiaolong Liu, Brandon L Fisher, Ulises Santiago, Jeffrey R Guest, et al. Synthesis of borophenes: Anisotropic, two-dimensional boron polymorphs. *Science*, 350(6267):1513–1516, 2015.
- [50] Baojie Feng, Jin Zhang, Qing Zhong, Wenbin Li, Shuai Li, Hui Li, Peng Cheng, Sheng Meng, Lan Chen, and Kehui Wu. Experimental realization of two-dimensional boron sheets. *Nature chemistry*, 8(6):563–568, 2016.
- [51] Marco Bernardi, Can Ataca, Maurizia Palummo, and Jeffrey C Grossman. Optical and electronic properties of two-dimensional layered materials. *Nanophotonics*, 6(2):479–493, 2017.
- [52] AH Castro Neto, Francisco Guinea, Nuno MR Peres, Kostya S Novoselov, and Andre K Geim. The electronic properties of graphene. *Reviews of modern physics*, 81(1):109, 2009.

- [53] AN Grigorenko, Marco Polini, and KS Novoselov. Graphene plasmonics. *Nature photonics*, 6(11):749–758, 2012.
- [54] Francesco Bonaccorso, Z Sun, TA Hasan, and AC Ferrari. Graphene photonics and optoelectronics. *Nature photonics*, 4(9):611, 2010.
- [55] Alexey B Kuzmenko, Erik Van Heumen, Fabrizio Carbone, and Dirk Van Der Marel. Universal optical conductance of graphite. *Physical review letters*, 100(11):117401, 2008.
- [56] Rahul Raveendran Nair, Peter Blake, Alexander N Grigorenko, Konstantin S Novoselov, Tim J Booth, Tobias Stauber, Nuno MR Peres, and Andre K Geim. Fine structure constant defines visual transparency of graphene. *Science*, 320(5881):1308–1308, 2008.
- [57] ZQ Li, Eric A Henriksen, Z Jiang, Zhao Hao, Michael C Martin, P Kim, HL Stormer, and Dimitri N Basov. Dirac charge dynamics in graphene by infrared spectroscopy. *Nature Physics*, 4(7):532–535, 2008.
- [58] Qiaoliang Bao, Han Zhang, Yu Wang, Zhenhua Ni, Yongli Yan, Ze Xiang Shen, Kian Ping Loh, and Ding Yuan Tang. Atomic-layer graphene as a saturable absorber for ultrafast pulsed lasers. *Advanced Functional Materials*, 19(19):3077–3083, 2009.
- [59] Xiaoming Sun, Zhuang Liu, Kevin Welsher, Joshua Tucker Robinson, Andrew Goodwin, Sasa Zaric, and Hongjie Dai. Nano-graphene oxide for cellular imaging and drug delivery. *Nano research*, 1(3):203–212, 2008.
- [60] Zhengtang Luo, Patrick M Vora, Eugene J Mele, AT Charlie Johnson, and James M Kikkawa. Photoluminescence and band gap modulation in graphene oxide. *Applied physics letters*, 94(11):111909, 2009.
- [61] Cinzia Casiraghi, Achim Hartschuh, Elefterios Lidorikis, Huihong Qian, Hayk Harutyunyan, Tobias Gokus, Kostya Sergeevich Novoselov, and AC Ferrari. Rayleigh imaging of graphene and graphene layers. *Nano letters*, 7(9):2711–2717, 2007.
- [62] Shi Wun Tong, Yu Wang, Yi Zheng, Man-Fai Ng, and Kian Ping Loh. Graphene intermediate layer in tandem organic photovoltaic cells. *Advanced Functional Materials*, 21(23):4430–4435, 2011.
- [63] Junbo Wu, Mukul Agrawal, Héctor A Becerril, Zhenan Bao, Zunfeng Liu, Yongsheng Chen, and Peter Peumans. Organic light-emitting diodes on solution-processed graphene transparent electrodes. *ACS nano*, 4(1):43–48, 2010.
- [64] Ming Liu, Xiaobo Yin, Erick Ulin-Avila, Baisong Geng, Thomas Zentgraf, Long Ju, Feng Wang, and Xiang Zhang. A graphene-based broadband optical modulator. *Nature*, 474(7349):64–67, 2011.
- [65] Feng Wang, Yuanbo Zhang, Chuanshan Tian, Caglar Girit, Alex Zettl, Michael Crommie, and Y Ron Shen. Gate-variable optical transitions in graphene. *science*, 320(5873):206–209, 2008.
- [66] Andrea Splendiani, Liang Sun, Yuanbo Zhang, Tianshu Li, Jonghwan Kim, Chi-Yung Chim, Giulia Galli, and Feng Wang. Emerging photoluminescence in monolayer mos₂. *Nano letters*, 10(4):1271–1275, 2010.
- [67] Tawinan Cheiwchanchamnangij and Walter RL Lambrecht. Quasiparticle band structure calculation of monolayer, bilayer, and bulk mos₂. *Physical Review B*, 85(20):205302, 2012.
- [68] Can Ataca, Hasan Sahin, and Salim Ciraci. Stable, single-layer mx₂ transition-metal oxides and dichalcogenides in a honeycomb-like structure. *The Journal of Physical Chemistry C*, 116(16):8983–8999, 2012.
- [69] JI A Wilson and AD Yoffe. The transition metal dichalcogenides discussion and interpretation of the observed optical, electrical and structural properties. *Advances in Physics*, 18(73):193–335, 1969.
- [70] A Chaves, JG Azadani, Hussain Alsaman, Diego Rabelo da Costa, R Frisenda, AJ Chaves, Seung Hyun Song, YD Kim, Daowei He, Jiadong Zhou, et al. Bandgap engineering of two-dimensional semiconductor materials. *npj 2D Materials and Applications*, 4(1):1–21, 2020.
- [71] Kin Fai Mak, Changgu Lee, James Hone, Jie Shan, and Tony F Heinz. Atomically thin mos₂: a new direct-gap semiconductor. *Physical review letters*, 105(13):136805, 2010.
- [72] Yi Zhang, Tay-Rong Chang, Bo Zhou, Yong-Tao Cui, Hao Yan, Zhongkai Liu, Felix Schmitt, James Lee, Rob Moore, Yulin Chen, et al. Direct observation of the transition from indirect to direct bandgap in atomically thin epitaxial mos₂. *Nature nanotechnology*, 9(2):111, 2014.
- [73] Weijie Zhao, Zohreh Ghorannevis, Lei Qiang Chu, Minglin Toh, Christian Kloc, Ping-Heng Tan, and Goki Eda. Evolution of electronic structure in atomically thin sheets of ws₂ and wse₂. *ACS nano*, 7(1):791–797, 2013.
- [74] Sidong Lei, Liehui Ge, Zheng Liu, Sina Najmaei, Gang Shi, Ge You, Jun Lou, Robert Vajtai, and Pulickel M Ajayan. Synthesis and photoresponse of large gap atomic layers. *Nano letters*, 13(6):2777–2781, 2013.
- [75] Lun Li, Zhong Chen, Ying Hu, Xuewen Wang, Ting Zhang, Wei Chen, and Qiangbin Wang. Single-layer single-crystalline snse nanosheets. *Journal of the American Chemical Society*, 135(4):1213–1216, 2013.
- [76] Babak Anasori, Maria R Lukatskaya, and Yury Gogotsi. 2d metal carbides and nitrides (mxenes) for energy storage. *Nature Reviews Materials*, 2(2):1–17, 2017.
- [77] Cory R Dean, Andrea F Young, Inanc Meric, Chris Lee, Lei Wang, Sebastian Sorgenfrei, Kenji Watanabe, Takashi Taniguchi, Phillip Kim, Kenneth L Shepard, et al. Boron nitride substrates for high-quality graphene electronics. *Nature nanotechnology*, 5(10):722–726, 2010.
- [78] Alessandro Lodesani, Andrea Picone, Alberto Brambilla, Dario Giannotti, Madan S Jagadeesh, Alberto Calloni, Gianlorenzo Bussetti, Giulia Berti, Maurizio Zani, Marco Finazzi, et al. Graphene as an ideal buffer layer for the growth of high-quality ultrathin cr₂o₃ layers on ni (111). *ACS nano*, 13(4):4361–4367, 2019.
- [79] Weiliang Ma, Pablo Alonso-González, Shaojuan Li, Alexey Y Nikitin, Jian Yuan, Javier Martín-Sánchez, Javier Taboada-Gutiérrez, Iban Amenabar, Peining Li, Saül Vélez, et al. In-plane anisotropic and ultra-low-loss polaritons in a natural van der waals crystal. *Nature*, 562(7728):557–562, 2018.
- [80] Patrick Vogt, Paola De Padova, Claudio Quaresima, Jose Avila, Emmanouil Frantzeskakis, Maria Carmen Asensio, Andrea Resta, Bénédicte Ealet, and Guy Le Lay. Silicene: compelling experimental evidence for graphenelike two-dimensional silicon. *Physical review letters*, 108(15):155501, 2012.

- [81] Linfei Li, Shuang-zan Lu, Jinbo Pan, Zhihui Qin, Yu-qi Wang, Yeliang Wang, Geng-yu Cao, Shixuan Du, and Hong-Jun Gao. Buckled germanene formation on pt (111). *Advanced Materials*, 26(28):4820–4824, 2014.
- [82] Zhili Zhu, Xiaolin Cai, Seho Yi, Jinglei Chen, Yawei Dai, Chunyao Niu, Zhengxiao Guo, Maohai Xie, Feng Liu, Jun-Hyung Cho, et al. Multivalency-driven formation of te-based monolayer materials: a combined first-principles and experimental study. *Physical review letters*, 119(10):106101, 2017.
- [83] Vidya Kochat, Atanu Samanta, Yuan Zhang, Sanjit Bhowmick, Praveena Manimunda, Syed Asif S Asif, Anthony S Stender, Robert Vajtai, Abhishek K Singh, Chandra S Tiwary, et al. Atomically thin gallium layers from solid-melt exfoliation. *Science advances*, 4(3): e1701373, 2018.
- [84] Jianping Ji, Xiufeng Song, Jizi Liu, Zhong Yan, Chengxue Huo, Shengli Zhang, Meng Su, Lei Liao, Wenhui Wang, Zhenhua Ni, et al. Two-dimensional antimonene single crystals grown by van der waals epitaxy. *Nature communications*, 7(1):1–9, 2016.
- [85] Rongting Wu, Ilya K Drozdov, Stephen Eltinge, Percy Zahl, Sohrab Ismail-Beigi, Ivan Božović, and Adrian Gozar. Large-area single-crystal sheets of borophene on cu (111) surfaces. *Nature nanotechnology*, 14(1):44–49, 2019.
- [86] Liang Fu and Charles L Kane. Superconducting proximity effect and majorana fermions at the surface of a topological insulator. *Physical review letters*, 100(9): 096407, 2008.
- [87] Constantine A Balanis. *Advanced engineering electromagnetics*. John Wiley & Sons, 2012.
- [88] Stefan A. Maier. *Plasmonics: Fundamentals and Applications*. Springer US, New York, NY, 2007. ISBN 978-0-387-33150-8. doi:10.1007/0-387-37825-1. URL <http://link.springer.com/10.1007/0-387-37825-1>.
- [89] Sergey G. Menabde, Daniel R. Mason, Evgeny E. Kornev, Changhee Lee, and Namkyoo Park. Direct Optical Probing of Transverse Electric Mode in Graphene. *Scientific Reports*, 6(1):21523, feb 2016. ISSN 2045-2322. doi:10.1038/srep21523. URL <http://www.nature.com/articles/srep21523>.
- [90] John Weiner and Frederico Nunes. *Light-matter Interaction: physics and engineering at the nanoscale*. Oxford University Press, 2017. ISBN 0198796676.
- [91] Chi H Lee. *Light-Matter Interaction: Atoms and Molecules in External Fields and Nonlinear Optics*. John Wiley & Sons, 2008.
- [92] Yu. V. Bludov, Aires Ferreira, N. M. R. Peres, and M. I. Vasilevskiy. A Primer On Surface Plasmon-Polaritons In Graphene. *International Journal of Modern Physics B*, 27(10):1341001, apr 2013. ISSN 0217-9792. doi:10.1142/S0217979213410014. URL <https://www.worldscientific.com/doi/abs/10.1142/S0217979213410014>.
- [93] F. Ramos-Mendieta, J. A. Hernández-López, and M. Palomino-Ovando. Transverse magnetic surface plasmons and complete absorption supported by doped graphene in Otto configuration. *AIP Advances*, 4(6):067125, jun 2014. ISSN 2158-3226. doi:10.1063/1.4883885. URL <http://aip.scitation.org/doi/10.1063/1.4883885>.
- [94] J. B. Pendry, L. Martín-Moreno, and F. J. Garcia-Vidal. Mimicking Surface Plasmons with Structured Surfaces. *Science*, 305(5685):847–848, aug 2004. ISSN 0036-8075. doi:10.1126/science.1098999. URL <https://www.sciencemag.org/lookup/doi/10.1126/science.1098999>.
- [95] Stefan A Maier, Mark L Brongersma, Pieter G Kik, Sheffer Meltzer, Ari A G Requicha, and Harry A Atwater. Plasmonics—a route to nanoscale optical devices. *Advanced materials*, 13(19):1501–1505, 2001.
- [96] Tony Low, Andrey Chaves, Joshua D Caldwell, Anshuman Kumar, Nicholas X Fang, Phaeton Avouris, Tony F Heinz, Francisco Guinea, Luis Martin-Moreno, and Frank Koppens. Polaritons in layered two-dimensional materials. *Nature materials*, 16(2):182–194, 2017.
- [97] Sergey A Mikhailov and Klaus Ziegler. New electromagnetic mode in graphene. *Physical review letters*, 99(1): 16803, 2007.
- [98] E H Hwang and S Das Sarma. Dielectric function, screening, and plasmons in two-dimensional graphene. *Physical Review B*, 75(20):205418, 2007.
- [99] George W Hanson. Dyadic Green’s functions and guided surface waves for a surface conductivity model of graphene. *Journal of Applied Physics*, 103(6):64302, 2008.
- [100] Marinko Jablan, Hrvoje Buljan, and Marin Soljačić. Plasmonics in graphene at infrared frequencies. *Physical review B*, 80(24):245435, 2009.
- [101] L A Falkovsky and A A Varlamov. Space-time dispersion of graphene conductivity. *The European Physical Journal B*, 56(4):281–284, 2007.
- [102] M Shoufie Ukhtary, Eddwi H Hasdeo, Ahmad R T Nugraha, and Riichiro Saito. Fermi energy-dependence of electromagnetic wave absorption in graphene. *Applied Physics Express*, 8(5):55102, 2015.
- [103] Charles Kittel, Paul McEuen, and Paul McEuen. *Introduction to solid state physics*, volume 8. Wiley New York, 1996.
- [104] Marinko Jablan, Marin Soljačić, and Hrvoje Buljan. Plasmons in graphene: fundamental properties and potential applications. *Proceedings of the IEEE*, 101(7): 1689–1704, 2013.
- [105] Hai-Yao Deng and Katsunori Wakabayashi. Retardation effects on plasma waves in graphene, topological insulators, and quantum wires. *Physical Review B*, 92(4):45434, 2015.
- [106] Ashkan Vakil and Nader Engheta. Transformation optics using graphene. *Science*, 332(6035):1291–1294, 2011.
- [107] M Shoufie Ukhtary, Ahmad RT Nugraha, Eddwi H Hasdeo, and Riichiro Saito. Broadband transverse electric surface wave in silicene. *Applied Physics Letters*, 109(6):063103, 2016.
- [108] Dror Sarid and William A Challener. *Modern introduction to surface plasmons: theory, mathematical modeling, and applications*. Cambridge University Press, 2010.
- [109] Xinyan Zhang, Hao Hu, Xiao Lin, Lian Shen, Baile Zhang, and Hongsheng Chen. Confined transverse-electric graphene plasmons in negative refractive-index systems. *npj 2D Materials and Applications*, 4(1):1–6, 2020.
- [110] Yuliy V Bludov, Daria A Smirnova, Yuri S Kivshar, NMR Peres, and Mikhail I Vasilevskiy. Nonlinear te-polarized surface polaritons on graphene. *Physical Re-*

- view B, 89(3):035406, 2014.
- [111] Giorgio Franceschetti. *Electromagnetics: theory, techniques, and engineering paradigms*. Springer Science & Business Media, 2013.
- [112] Robert E Collin. *Foundations for microwave engineering*. John Wiley & Sons, 2007.
- [113] Cole B Reynolds, M Shoufie Ukhtary, and Riichiro Saito. Absorption of THz electromagnetic wave in two mono-layers of graphene. *Journal of Physics D: Applied Physics*, 49(19):195306, 2016.
- [114] AL-Ghezi Hammid, Rudra Gnawali, Partha P Banerjee, Lirong Sun, Jonathan Slagle, and Dean Evans. 2×2 anisotropic transfer matrix approach for optical propagation in uniaxial transmission filter structures. *Optics Express*, 28(24):35761–35783, 2020.
- [115] Tianrong Zhan, Xi Shi, Yunyun Dai, Xiaohan Liu, and Jian Zi. Transfer matrix method for optics in graphene layers. *Journal of Physics: Condensed Matter*, 25(21):215301, 2013.
- [116] Matteo Bruno Lodi, Nicola Curreli, Alessandro Fanti, Claudia Cuccu, Danilo Pani, Alessandro Sanginario, Andrea Spanu, Paolo Motto Ros, Marco Crepaldi, Danilo Demarchi, et al. A periodic transmission line model for body channel communication. *IEEE Access*, 8:160099–160115, 2020.
- [117] Bahaa E. A. Saleh and Malvin Carl Teich. *Fundamentals of Photonics*, volume 5 of *Wiley Series in Pure and Applied Optics*. John Wiley & Sons, Inc., New York, USA, aug 1991. ISBN 0471839655. doi: 10.1002/0471213748. URL <http://doi.wiley.com/10.1002/0471213748>.
- [118] WT Welford. The principles of nonlinear optics. *Physics Bulletin*, 36(4):178, 1985.
- [119] Robert Boyd. *Nonlinear Optics*. Elsevier, 3rd edition, 2008. ISBN 9780080485966.
- [120] Cristian Manzoni and Giulio Cerullo. Design criteria for ultrafast optical parametric amplifiers. *Journal of Optics*, 18(10):103501, 2016.
- [121] JE Sipe, DJ Moss, and HM Van Driel. Phenomenological theory of optical second-and third-harmonic generation from cubic centrosymmetric crystals. *Physical Review B*, 35(3):1129, 1987.
- [122] Chiara Trovatiello, Andrea Marini, Xinyi Xu, Changhan Lee, Fang Liu, Nicola Curreli, Cristian Manzoni, Stefano Dal Conte, Kaiyuan Yao, Alessandro Ciattoni, et al. Optical parametric amplification by monolayer transition metal dichalcogenides. *Nature Photonics*, 15(1):6–10, 2021.
- [123] Jiangang He, Kerstin Hummer, and Cesare Franchini. Stacking effects on the electronic and optical properties of bilayer transition metal dichalcogenides MoS 2, MoSe 2, WS 2, and WSe 2. *Physical Review B - Condensed Matter and Materials Physics*, 89(7):075409, feb 2014. ISSN 10980121. doi:10.1103/PhysRevB.89.075409. URL <https://journals.aps.org/prb/abstract/10.1103/PhysRevB.89.075409>.
- [124] Yilei Li, Yi Rao, Kin Fai Mak, Yumeng You, Shuyuan Wang, Cory R. Dean, and Tony F. Heinz. Probing symmetry properties of few-layer MoS2 and h-BN by optical second-harmonic generation. *Nano Letters*, 13(7):3329–3333, jul 2013. ISSN 15306984. doi:10.1021/nl401561r. URL <https://pubs.acs.org/sharingguidelines>.
- [125] Nardeep Kumar, Sina Najmaei, Qiannan Cui, Frank Ceballos, Pulickel M Ajayan, Jun Lou, and Hui Zhao. Second harmonic microscopy of monolayer mos 2. *Physical Review B*, 87(16):161403, 2013.
- [126] Mervin Zhao, Ziliang Ye, Ryuji Suzuki, Yu Ye, Hanyu Zhu, Jun Xiao, Yuan Wang, Yoshihiro Iwasa, and Xiang Zhang. Atomically phase-matched second-harmonic generation in a 2d crystal. *Light: Science & Applications*, 5(8):e16131–e16131, 2016.